Investigating the influence of the counter Si-cell on the optoelectronic performance of high-efficiency monolithically perovskites/silicon tandem cells under various optical sources[*]

Moustafa Ganoub[1], Sameh O. Abdellatif[2]**, Khaled Kirah[3], and Hani A. Ghali[2]**

1. The Renewable Energy Postgraduate Programme and the FabLab in the Centre for Emerging Learning Technologies (CELT), The British University in Egypt (BUE), Cairo 11837, Egypt

2. FabLab in the Centre for Emerging Learning Technologies (CELT), Electrical Engineering Department, Faculty of Engineering, The British University in Egypt (BUE), Cairo 11837, Egypt

3. Engineering Physics Department, Faculty of Engineering, Ain Shams University, Cairo, Egypt

Nowadays, tandem structures have become a valuable competitor to conventional silicon solar cells, especially for perovskite over silicon, as metal halides surpassed Si with tunable bandgaps, high absorption coefficient, low deposition, and preparation costs. This led to a remarkable enhancement in the overall efficiency of the whole cell and its characteristics. Consequently, this expands the usage of photovoltaic technology in various fields of applications not only under conventional light source spectrum in outdoor areas, i.e., AM1.5G, but also under artificial light sources found indoors with broadband intensity values, such as Internet of things (IoTs) applications to name a few. We introduce a numerical model to analyze perovskite/Si tandem cells (PSSTCs) using both crystalline silicon (c-Si) and hydrogenated amorphous silicon (a-Si: H) experimentally validated as base cells. All proposed layers have been studied with *J-V* characteristics and energy band diagrams under AM1.5G by using SCAPS-1D software version 3.7.7. Thereupon, the proposed architectures were tested under various artificial lighting spectra. The proposed structures of $Li_4Ti_5O_{12}/CsPbCl_3/MAPbBr_3/CH_3NH_3PbI_3/Si$ recorded a maximum power conversion efficiency (PCE) of 25.25% for c-Si and 17.02% for a-Si: H, with nearly 7% enhancement concerning the Si bare cell in both cases.

Several light-harvesting systems have evolved during the last few decades[1], with various power-scale applications[2] in mind. In theory, a light-harvesting system may be shown using three primary components: the light spectrum to be captured, the light harvester, and the electrical load to be powered. Most of the time, outdoor solar panels and modules fabricated from Si or any other elemental or compound semiconductor[3] are used to harvest the AM1.5G solar spectrum. Si-based modules are extensively used in such applications owing to the availability of the material, the competitive market price, and its bang-gap energy matching with the solar spectrum[4]. However, the input light spectrum influenced the design parameters of the light harvester[5]. In space applications, for instance, light harvesters are tailored for the AM0 spectrum[6]. Alternately, indoor light harvesters[1,5] are developed for artificial illumination spectra, such as light-emitting diode (LED)[7], halogen lamps[8], xenon lamps[9], and laser[10]. Such diversity enables researchers to design light harvesters to enhance photon utilization[11].

Perovskites have recorded a growing trend in effectively harvesting photons as an absorbing layer[11-13], which places them at the forefront of a broad spectrum of semiconductors capable of being incorporated as an active layer in light harvesters. In one-fourth of the research published[14], perovskite solar cell has been studied and introduced. This puts it close to the theoretical limit of Si-based solar cells, around 31%. Perovskite-based solar cells have the additional property of being able to tune their energy bandgap[15], which enables them to collect a broad range of different light spectra. This is an extra benefit of these cells. Because of this, perovskite has shown significant promise in bifacial cells, semi-transparent light harvesters, and indoor light harvesting[1,5]. Previous efforts[16] to create a semi-transparent bifacial cell using perovskite solar cells exhibited an intriguing trade-off between the cells' transparency

and efficiency.

Along the same perspective, towards maximizing the efficiency of power conversion, the architecture of multi-junction solar cells, also known as tandem cells, demonstrated an efficiency above 40%[17]. The tandem cells are meant to integrate successive cascaded absorbing layers, optically structured to gather as many incoming photons as feasible[18]. In tandem cells, the layer arrangement is a crucial design element, often referred to as bandgap engineering[19].

The most promising tandem cell configuration is silicon-perovskite heterojunction[20]. Perovskites, which have a bandgap of more than 1.6 eV, are used as a front layer to absorb low-wavelength photons. This is accompanied by a perfect visible absorber, Si, with a bandgap of 1.12 eV. So, different reports[18-20] have shown different topologies for perovskite/silicon tandem cells (PSSTCs). Numerical simulations are often used to determine how perovskite/Si multi-junction should be made[21]. One of the most important things to consider when designing is controlling the light within the tandem cell by arranging the heterostructures[22]. On the other hand, optoelectronic numerical models have shown high predictions that are better than 40% efficient[23]. Experiments have shown that the overall efficiency of power conversion is above 30%[24].

Our work in this study is to investigate the proposed tandem structure PSSTC numerically under various lighting spectra for indoor and outdoor applications by using both crystalline silicon (c-Si) and hydrogenated amorphous silicon (a-Si: H) as base cells interchangeably with the same pervo structure deposited. In both topologies, the Si solar cell under AM1.5G is the bare operating condition for trading between both arrangements. The *J-V* characteristic curves and the energy-band diagrams have been conducted in the optoelectronic numerical model for each cell. Moreover, the interpretational analysis is combined with experimental validation points from the literature.

As stated in earlier, the present work uses PSSTCs exposed optically to various artificial illumination spectra. As our bare cell, we considered both p-i-n (a-Si: H) and p^{++}-n-n^{++} (c-Si) junctions (see schematic in Fig.1(a) and (b)), with design parameters tabulated in Tabs.1 and 2. Our simulated model is based on the experimental Si-based cell described in Refs.[25—27] respectively. Both Si-based cells, on the other hand, will be topped with the same perovskite, ABX_3 structural-based materials. Each layer has been merged separately so that its optoelectronic effects may be analyzed (see the schematic in Fig.1(c)—(f)). The selected perovskites are lithium titanate ($Li_4Ti_5O_{12}$), barium titanate ($BaTiO_3$), cesium lead chloride ($CsPbCl_3$), me-thylammonium lead tribromide ($MAPbBr_3$), and methylammonium lead halide ($CH_3NH_3PbI_3$)[28-30]. The configuration of the layers is controlled following the optical energy bandgap, starting with 1.6 eV for $CH_3NH_3PbI_3$ just over the Si cell and ending by the top layer facing light spectrum 3.4 eV and 3.55 eV for both $BaTiO_3$ and $Li_4Ti_5O_{12}$ interchangeably. Another critical parameter in the design of the tandem cells is the current matching. Generally, tandem cell current is limited by the cell that produces lower current. The cell that could, in principle, produce higher current, is limited to this low current, and operates at a voltage above its maximum power point. This means the voltage of the tandem cell increases slightly but this in no way compensates the large efficiency loss arising from the lower tandem cell current. We addressed this point later as a part of the results interpretation.
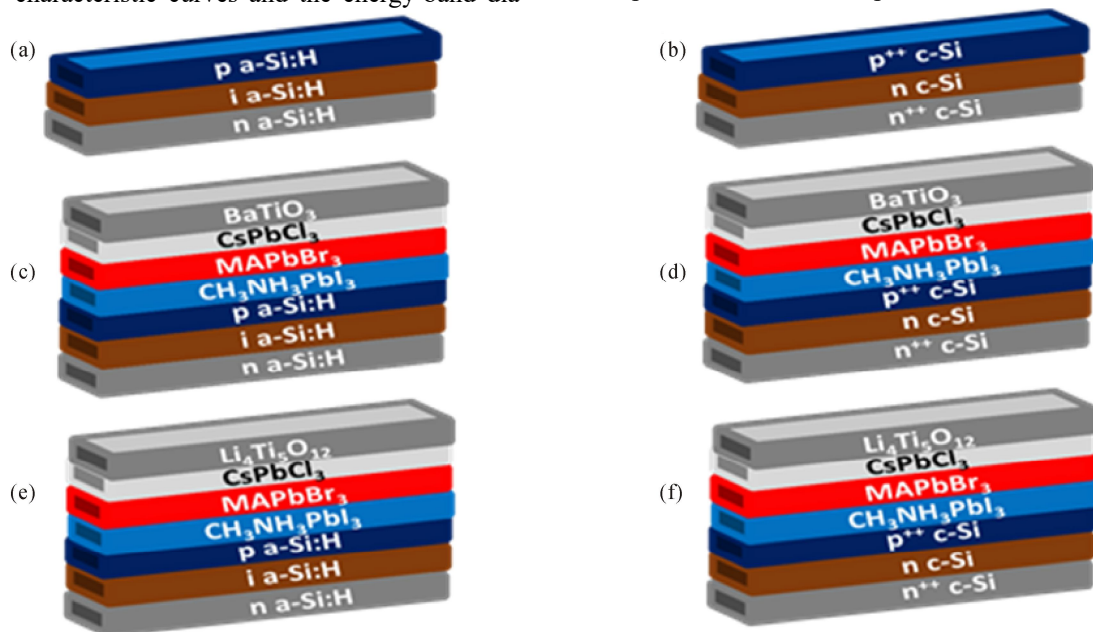

Fig.1 Schematics for (a) bare a-Si: H based cell, (b) BaTiO₃/CsPbCl₃/MAPbBr₃/CH₃NH₃PbI₃/a-Si: H cell, (c) Li₄Ti₅O₁₂/CsPbCl₃/MAPbBr₃/CH₃NH₃PbI₃/a-Si: H cell, (d) bare c-Si-based cell, (e) BaTiO₃/CsPbCl₃/MAPbBr₃/CH₃NH₃PbI₃/c-Si cell, and (f) Li₄Ti₅O₁₂/CsPbCl₃/MAPbBr₃/CH₃NH₃PbI₃/c-Si cell

Tab.1 Input material parameters for the a-Si: H bare cell (The cell was selected to represent the experimental work described in Refs.[25—27])

	p a-Si: H	i a-Si: H	n a-Si: H
Thickness (μm)	0.009	0.5	0.02
Concentration (cm^{-3})	N_A=1.00× 10^{12}	N_D=1.00× 10^{10}	N_D=1.00× 10^{11}

Tab.2 Input material parameters for the c-Si bare cell (The cell was selected to represent the experimental work reported in Ref.[27])

	n^{++} c-Si	n c-Si	p^{++} c-Si
Thickness (μm)	0.05	220	0.1
Concentration (cm^{-3})	N_D=8.75× 10^{17}	N_D=2.00× 10^{14}	N_A=1.70× 10^{16}

Specifically, all suggested configurations for optical injection were modeled using the typical sun spectrum of AM1.5G (Fig.2). To imitate natural illumination, cells were exposed to various artificial lighting spectra, such as xenon lamp, LEDs, metal halide, and high-power laser sources with changeable resonance over 400 nm to 1 000 nm. Fig.2 shows a plot of every spectral power density and a sample from a high-power laser (166 W/m^2 peaks) at 600 nm. All the suggested architectural designs were numerically simulated using SCAPS under the chosen light spectra.

In the first place, validating both models were done by using experimentally fabricated bare cells[25-27], through modeling each via the SCAPS simulation tool. As a result, the bare cells were topped layer by layer, and each was tested and studied under AM1.5G separately. This was followed afterward by variating optoelectronic performance under several optical injection resources studied. Simulating the *J-V* characteristic of both a-Si: H and c-Si bare cells under AM1.5G was our initial step in validating our proposed models through their optoelectronic structures (see Fig.3, plot (a) and (b)). The a-Si: H simulated data from our model to the experimental data recorded a 6% deviation, in Ref.[26], for the short-circuit current density reaching 17.163 mA/cm^2 numerically and 18.3 mA/cm^2 experimentally. However, it was almost the same in the c-Si model as the simulated data recorded showed the same measured output value in Ref.[27] for the short-circuit current density reaching 38.6 mA/cm^2. For both cells validation, the simulated data recorded a slight deviation around 1.32% and 2.39% in the measured values of the open-circuit voltages in a-Si: H and c-Si respectively, reaching 831 mV numerically and 820 mV experimentally for a-Si: H as in Refs.[23] and [24], and reaching 612 mV numerically and 627 mV experimentally as in Ref.[25] for c-Si.

The given a-Si: H-bare cell determined an overall

power conversion efficiency of 10.51% in our simulated model and 10.3% in the experimental results, with 2% difference between both readings, and 18.9% experimentally and 18.6% numerically, with 1.5% deflection from the laboratory data. It is important to note that both Si bare cells have been selected as reference cells since they are previously manufactured, as stated in the literature and can be coated with perovskite films[25-27].
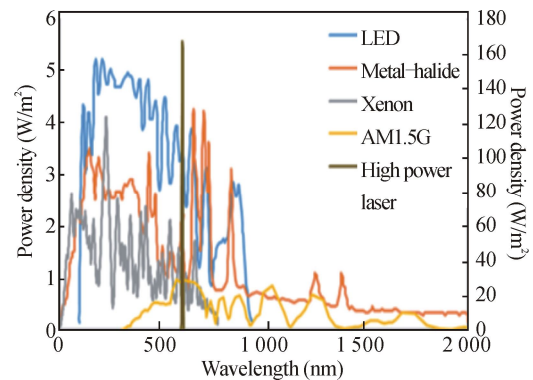

Fig.2 Power spectral density for all light sources (LED, metal-halide, and xenon are plotted with respect to the primary vertical axis to the left, while AM1.5G and high-power laser sources are plotted with respect to the secondary vertical axis to the right)

To capture the most photons from the incident source, tandem cells are often built together in a multi-junction structure. The bandgap is narrowed from the top electrode, the side of the higher band, to the substrate junction, which is often the primary design element in tandem cells. Under the AM1.5G c-Si bare cell recorded higher efficiency than the a-Si: H[27,28], as mentioned in the previous section. This could be explained based on the crystalline structures for both bare cells, as the c-Si lattice composition surpasses the a-Si: H due to its homogenous arrangement, which facilitates the formation and transportation of electron-hole pairs generated by photons absorption, and this reflects directly on the optoelectrical conversion efficiency. In the same path, structural defects in the a-Si: H due to the hydrogenation process result in recombination centers, causing carrier lifetime to be shortened, and transporting the charge carriers from one side to another will be transported a significant challenge, which, in conclusion, results in lower power conversion efficiency (PCE) in the case of a-Si: H.

On the other hand, the inhomogeneity of the a-Si: H structure gives it a significant advantage over c-Si as the absorption coefficient of a-Si: H is higher with an order of magnitude than c-Si in photon absorption with energy more than 1.8 eV. Accordingly, the absorbed light will face more internal scattering in the non-crystalline structure than the crystalline ones, leading to efficient absorption of light by the a-Si: H and less material usage under the same incident light in comparison with c-Si, therefore a-Si solar cell will respond efficiently over the c-Si solar cell under indoor applications. By adding our proposed

pervo materials, Fig.1(c) and (e), the overall recorded PCE in both cases was 12.93% with a 2.42% increase from its bare cell. Also, for the arrangements in Fig.1(d) and (f), the overall PCE recorded was 23.6% with 4.94% increase over the bare cell efficiency. Topping both bare cells with comprehensive bandgap pervo material enhances the pho-

ton capturing from the solar spectrum by broadening the wavelength/frequency range. The open circuit voltage (V_{oc}) recorded a remarkable overall increase of 15.5% with both c-Si arrangements (Fig.3 plot (d) and (f)) with respect to c-Si bare cell (Fig.3 plot (b)) with a neglected increase in the whole cell short circuit current (J_{sc}).

Tab.3 Input material parameters for the top perovskite layers used in the tandem cell ($Li_4Ti_5O_{12}$, $BaTiO_3$, $CsPbCl_3$, $MAPbBr_3$ and $CH_3NH_3PbI_3$ data are captured from Refs.[28—30])

| Material/Parameter	$Li_4Ti_5O_{12}$	$BaTiO_3$	$CsPbCl_3$	$MAPbBr_3$	$CH_3NH_3PbI_3$
Bandgap (eV)	3.55	3.4	2.99	2.3	1.6
Electron affinity (eV)	3.6	3.76	3.77	3.85	3.9
Dielectric permittivity	14.1	19	2.513	20.5	6.5
CB effective density of states (cm^{-3})	2.84×10^{19}	2.84×10^{19}	1.00×10^{21}	2.2×10^{18}	2.20×10^{18}
VB effective density of states (cm^{-3})	1.84×10^{19}	1.84×10^{19}	2.00×10^{20}	1.80×10^{19}	1.80×10^{19}
Electron mobility (cm²/Vs)	1.00×10^{2}	1.30×10^{-1}	1.30×10^{2}	8.60	2.00
Hole mobility (cm²/Vs)	1.00×10^{2}	8.00×10^{-2}	1.90×10^{2}	9.00	2.00
Acceptor concentration (cm^{-3})	1.00×10^{19}	1.00×10^{22}	1.00×10^{22}	1.00×10^{22}	1.00×10^{22}
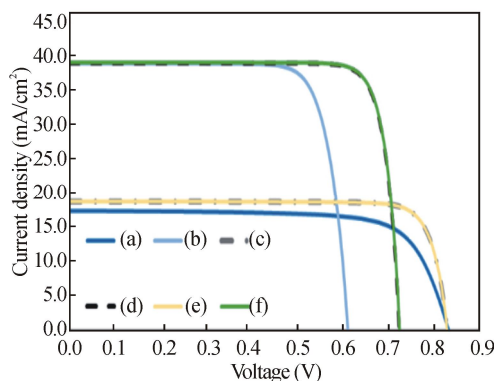
Fig.3 *J-V* characteristics for the proposed solar cell architectures under AM1.5G: (a) Bare a-Si: H based cell, (b) $BaTiO_3/CsPbCl_3/MAPbBr_3/CH_3NH_3PbI_3/$a-Si: H tandem cell; (c) $Li_4Ti_5O_{12}/CsPbCl_3/MAPbBr_3/CH_3NH_3PbI_3/$a-Si: H tandem cell; (d) Bare c-Si-based cell; (e) $BaTiO_3/CsPbCl_3/MAPbBr_3/CH_3NH_3PbI_3/$c-Si tandem cell; (f) $Li_4Ti_5O_{12}/CsPbCl_3/MAPbBr_3/CH_3NH_3PbI_3/$c-Si cell

On the contrary, for the a-Si: H arrangements, the noticeable overall change was in the short circuit current (J_{sc}) Fig.3 plot (c) and (e) versus Fig.3 plot (a), showing a 7.7% enhancement for the whole cell. Both cell arrangements have a negligible overall decrease in the open circuit voltage (V_{oc}). The enhancement of V_{oc} and J_{sc} in both c-Si and a-Si: H, respectively, directly reflects on the whole structure fill factor (FF) with a rise of 5.13% and 10.2% compared to both bare cells.

By testing both bare cells under the artificial light sources introduced in Fig.2, it was noticed that the a-Si: H bare cell has higher efficiency under LED and halide

optical source (Fig.4 plot (a), Fig.5 plot (a)), recording PCE of 14.34% and 11.31% respectively in comparison with the bare cell under normal lighting conditions (Fig.3 plot (a)) with a rise of 4% and 1% under each source. And nearly the same PCE under xenon light source (Fig.6 plot (a)). On the other hand, c-Si bare cells under the same artificial sources recorded PCEs of 16.6%, 17.92%, and 19.93% under LED (Fig.4 plot (b)), halide (Fig.5 plot (b)), and xenon (Fig.6 plot (b)) respectively with 2% reduction in the output efficiency under LED and nearly 0.75% under halide optical injection cases, and a rise of 1.5% under xenon all in comparison with c-Si bare cell PCE output under the standard sunlight source. Moreover, this goes back for several reasons combined, firstly is the bandgap of both bare cells 1.55 eV to 2.1 eV or 1.03 eV to 1.89 eV in the case of a-Si: H and 1.12 eV in case of c-Si, secondly the optical source spectrum shift and lastly the structure of both materials. Backing to the *J-V* curves in Fig.3, both BaTiO_3 and Li_4Ti_5O_{12} configurations layered on the c-Si (Fig.1(d) and (f)) and a-Si: H (Fig.1(c) and (e)) recorded the same PCE of 23.6% and 12.9% respectively under standard conditions of the one sun AM1.5G, with 2.2% improvement in the case of a-Si: H and 5% in the case of c-Si, which is an expected enhancement under one sun for the c-Si side for its bandgap and homogenous crystalline structure.

Regarding the suggested PSSTCs, all the other perovskite top junctions have a reasonably large bandgap with respect to Si. Therefore, perovskites with these bandgap ranges can capture photons with higher frequencies, particularly those in the spectrum's blue, violet, and ultraviolet regions. This explains the same performance

found in Figs.4, 5 and 6 since the ultra-violet part of the AM1.5G is not dominant, as shown in Fig.2. Therefore, infusing these topologies with an ultra-violet-biased light spectrum should benefit the captured current. In addition, both tandem structures were tested under monochromatic laser source with variable wavelengths in Figs.7 and 8, respectively. It is important to highlight that the higher power laser sources utilized here are adjusted in terms of intensity to avoid any material damage. Moreover, the deep ultra-violet laser below 350 nm is not utilized here to protect the cells from any high energy photons. In Fig.8, a-Si tandem structure was tested up to 600 nm laser to eliminate any structural failure.
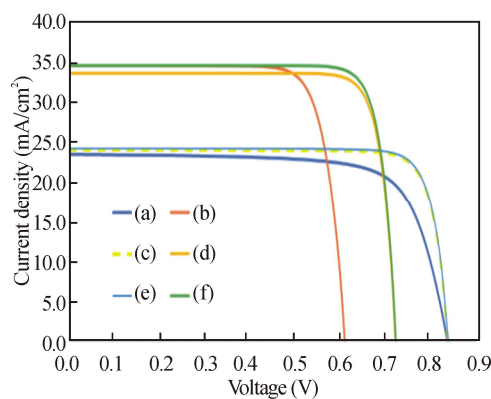

Fig.4 *J-V* characteristics for the proposed solar cell architectures under LED (Following the same sequence in Fig.3)
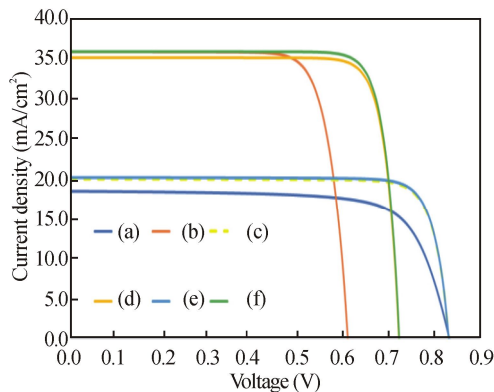

Fig.5 *J-V* characteristics for the proposed solar cell architectures under metal halide (Following the same sequence in Fig.3)

The ultraviolet portion of the electromagnetic spectrum predominates in artificial lightings, such as in the case of the metal halide, LED, and xenon light sources whose spectra are depicted in Fig.2. As a result, we evaluated how effectively these three different light sources performed with each of the four proposed designs, as seen in Fig.1(c)—(f). In general, the open-circuit voltage did not display any noticeable changes in the AM1.5G condition. Simultaneously, the short-circuit current varies within the same order of

magnitude, with improved performance under LED injection for a-Si: H base cell and xenon injection for c-Si. Under the three artificial light sources, the performance of the BaTiO$_3$ structure might be marginally improved by switching to the lithium titanate structure. This is because lithium titanate has a bandgap of 3.55 eV.

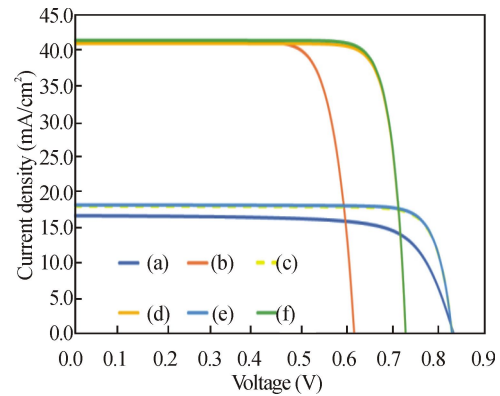**Fig.6 *J-V* characteristics for the proposed solar cell architectures under xenon (Following the same sequence in Fig.3)**

In contrast, BaTiO$_3$ only has a bandgap of 3.4 eV. for the c-Si deposited by lithium titanate configuration (Fig.1(f)), the maximum PCE recorded under the xenon optical source was 25.25% which overcame the corresponding PCE under AM1.5G by nearly 3%. However, the same configuration (Fig.1(e)) under the LED optical source deposited on the a-Si: H has recorded 17.02% maximum PCE with 5% more than the PCE recorded for the same case under AM1.5G. Furthermore, both the 25.25% and 17.02% can be compared with both Si base cells under the xenon and LED injections, respectively, for each case which was recorded at 19.3% for c-Si and 14.34% in a-Si: H, resulting in more than 6% and 3% enhancement.

Testing both structure configurations in Fig.1(c)—(f) under various high-power laser sources wavelengths, the output efficiencies raised dramatically, reaching 50.5% in both c-Si-based cells and 31.1% in both a-Si: H-based cells configurations. The a-Si: H models gave no output under long wavelengths due to a relatively high bandgap over the whole structure, which completely blocks these wavelengths.

It is worth to highlight that however the proposed structures enhanced the overall tandem efficiency of the cell, but the maximum recoded efficiencies are still below the thermotical limit of Si-0 based cells. The below limit efficiencies reported here is a factor of the bare cell efficiencies itself. We chose to build our tandem structure on Si-based cell which have already been fabricated in the literature to enable experimental validation for our proposed model. Alternatively, such experimentality fabricated cells showed relatively low efficiencies (around 17.02%) with respect to the theoretical limit. That's justify the 25.25% maximum efficiency reported.

However, by alternating the bare cell with another higher efficiency, the overall tandem cell efficiency can exceed the 30% limit of Si. We consider this as a part of the future work.
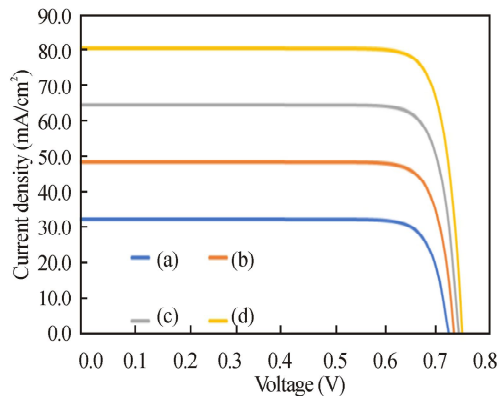

Fig.7 *J-V* characteristics for the proposed solar cell architectures BaTiO$_3$ or Li$_4$Ti$_5$O$_{12}$/CsPbCl$_3$/MAPbBr$_3$/ CH$_3$NH$_3$PbI$_3$/c-Si tandem cell under laser: (a) 400 nm; (b) 600 nm; (c) 800 nm; (d) 1 000 nm
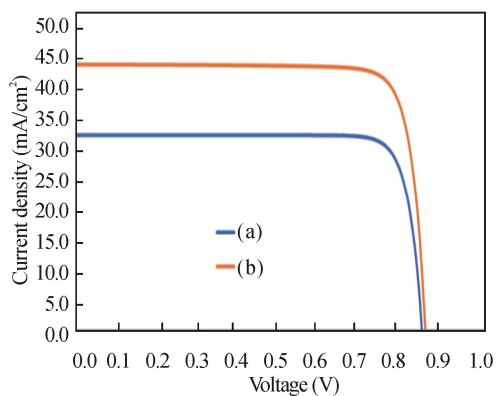
Fig.8 *J-V* characteristics for the proposed solar cell architectures BaTiO$_3$ or Li$_4$Ti$_5$O$_{12}$/CsPbCl$_3$/MAPbBr$_3$/ CH$_3$NH$_3$PbI$_3$/a-Si tandem cell under laser: (a) 400 nm; (b) 600 nm

In conclusion, Si-based cells have exhibited a steady, reasonably high PCE. Nevertheless, multi-junction cells provide the prospect of changing the PCE theoretical limit. This is relevant to the situation. In such tandem designs, materials with broader bandgaps are used as a front junction to broaden the cells' absorption spectrum. In addition, the formation of an extended transport layer for either electrons or holes is facilitated by adding these layers. In our construction, CH$_3$NH$_3$PbI$_3$ plays an essential role in increasing the open-circuit voltage of the tandem configuration deposited on both c-Si and a-Si: H to a value of 0.74 V and 0.85 V. This is the maximum value that can be achieved with such a topology under these light sources. In addition, CsPbCl$_3$/MAPbBr$_3$ perovskites were used to boost the current density that was collected and get it closer to the bounds of 40 mA/cm^2 in the c-Si and 25 mA/cm^2 in the a-Si: H structures, respectively.

Herein, the nearly matching of the current between the sub-cells ensures the appropriate current matching of the tandem structure. Finally, the LED spectrum showed the greatest computability with the a-Si: H tandem structure, achieving an overall PCE of 17.02% in comparison with all other optical sources used, and on the other hand, the xenon spectrum demonstrated the highest computability with the c-Si tandem structure, achieving an overall PCE of 25.25% among all other light sources.

Statements and Declarations

The authors declare that there are no conflicts of interest related to this article.

References

[1]   WANG T, WEN Z, XU L H, et al. One-micron-thick organic indoor light harvesters with low photocurrent loss and fill factors over 67%[J]. Journal of materials chemistry A, 2021, 23(9)：13515-13521.

[2]   HATEM T, ISMAIL Z, ELMAHGARY M G, et al. Optimization of organic meso-superstructured solar cells for underwater IoT² self-powered sensors[J]. IEEE transactions on electron devices, 2021, 68(10)： 5319-5321.

[3]   ABDELLATIF S, GHANNAM R, KHALIL A S G. Simulating the dispersive behavior of semiconductors using the Lorentzian & Drude model for photovoltaic devices[J]. Applied optics, 2014, 53：3294-3300.

[4]   ANDREANI L C, BOZZOLA A, KOWALCZEWSKI P, et al. Silicon solar cells：toward the efficiency limits[J]. Advances in physics：X, 2019, 4：1548305.

[5]   MATHEWS I, KING P J, STAFFORD F, et al. Performance of III-V solar cells as indoor light energy harvesters[J]. IEEE journal of photovoltaics, 2015, 6： 230-235.

[6]   SAYRE L, CAMARILLO A E, PEARCE P, et al. Ultra-thin GaAs solar cells with nanophotonic metal-dielectric diffraction gratings fabricated with displacement Talbot lithography[J]. Progress in photovoltaics：research and applications, 2022, 30：96-108.

[7]   MINNATULLAH M H, ANWAR S, SAMEH O A, et al. Toward low-cost, stable, and uniforhigh-power LED array for solar cells characterization[J]. Proc. SPIE, 2020：11496.

[8]   OJANEN M, KÄRHÄ P, IKONEN E. Spectral irradiance model for tungsten halogen lamps in 340-850 nm wavelength range[J]. Applied optics, 2010, 49：880.

[9]   LEARY G, SWITZER G, KUNTZ G, et al. Comparison of xenon lamp-based and led-based solar simulators[C]//2016 IEEE 43rd Photovoltaic Specialists Conference (PVSC), June 5-10, 2016, Portland, OR, USA. New York：IEEE, 2016：3062-3067.

[10]   BERG-SØRENSEN K, PETERMAN E J, WEBER T, et al. Power spectrum analysis for optical tweezers. II：

laser wavelength dependence of parasitic filtering, and how to achieve high bandwidth[J]. Review of scientific instruments, 2006, 77：063106.

[11]   MAHRAN A M, ABDELLATIF S O. Optoelectronic modelling and analysis of transparency against efficiency in perovskites/dye-based solar cells[C]. 2022 International Conference on Microelectronics (ICM), December 4-7, 2022, Casablanca, Morocco. New York：IEEE, 2022：178-181.

[12]   EID A A, ISMAIL Z S, ABDELLATIF S O. Optimizing SCAPS model for perovskite solar cell equivalent circuit with utilizing Matlab-based parasitic resistance estimator algorithm[C]//2020 2nd Novel Intelligent and Leading Emerging Sciences Conference (NILES), October 24-26, 2020, Giza, Egypt. New York：IEEE, 2020：503-507.

[13]   CHOI W, SONG S W, HAN S G, et al. The origin of photoinduced capacitance in perovskite solar cells：beyond ionic-to-electronic current amplification[J]. Advanced electronic materials, 2020：2000030.

[14]   KIM G H, KIM D S. Development of perovskite solar cells with> 25% conversion efficiency[J]. Joule, 2021, 5：1033-1035.

[15]   HU Z, LIN Z, SU J, et al. A review on energy band-gap engineering for perovskite photovoltaics[J]. Solar RRL, 2019, 3：1900304.

[16]   HASSAN M M, ISMAIL Z S, HASHEM E M, et al. Investigating the tradeoff between transparency and efficiency in semitransparent bifacial mesosuperstructured solar cells for millimeter-scale applications[J]. IEEE journal of photovoltaics, 2021, 11(5)：1222-1235.

[17]   KIM K, GWAK J, AHN S K, et al. Simulations of chalcopyrite/c-Si tandem cells using SCAPS-1D[J]. Solar energy, 2017, 145：52-58.

[18]   FU F, LI J, YANG T C, et al. Monolithic perovskite-silicon tandem solar cells：from the lab to fab[J]. Advanced materials, 2022, 34：2106540.

[19]   TODOROV T, GERSHON T, GUNAWAN O, et al. Monolithic perovskite-CIGS tandem solar cells via in situ band gap engineering[J]. Advanced energy materials, 2015, 5：1500799.

[20]   ALBRECHT S, SALIBA M, BAENA J P C, et al. Monolithic perovskite/silicon-heterojunction tandem solar cells processed at low temperature[J]. Energy & environmental science, 2016, 9：81-88.

[21]   LEHR J, LANGENHORST M, SCHMAGER R, et al. Energy yield modelling of perovskite/silicon two-terminal tandem PV modules with flat and textured interfaces[J]. Sustainable energy & fuels, 2018, 2：2754-2761.

[22]   JACOBS D A, LANGENHORST M, SAHLI F, et al. Light management：a key concept in high-efficiency perovskite/silicon tandem photovoltaics[J]. The journal of physical chemistry letters, 2019, 10：3159-3170.

[23]   HASAN M, HABIB M, MATIN M, et al. Modeling of high efficient perovskite-Si tandem solar cell[C]//2017 3rd International Conference on Electrical Information and Communication Technology (EICT), December 7-9, 2017, Khulna, Bangladesh. New York：IEEE, 2017：1-5.

[24]   SHEN H, WALTER D, WU Y, et al. Monolithic perovskite/Si tandem solar cells：pathways to over 30% efficiency[J]. Advanced energy materials, 2020, 10：1902840.

[25]   AYAT L, NOUR S, MEFTAH A. Comparative study of a PIN homojunction a-Si：H solar cell[J]. Journal of ovonic research, 2019, 15(1)：89-94.

[26]   SCHROPP R E, SCHÜTTAUF J W, VAN DER WERF K. Oxygenated protocrystalline silicon thin films for wide bandgap solar cells[J]. MRS online proceedings library (OPL), 2010, 1245：203.

[27]   SCHMIGA C, NAGEL H, SCHMIDT J. 19% efficient n-type Czochralski silicon solar cells with screen-printed aluminium-alloyed rear emitter[J]. Progress in photovoltaics：research and applications, 2006, 14：533-539.

[28]   MORSI M A, ABDELAZIZ M, ORABY A H, et al. Effect of lithium titanate nanoparticles on the structural, optical, thermal and electrical properties of polyethylene oxide/carboxymethyl cellulose blend[J]. Journal of materials science：materials in electronics, 2018, 29(18)：15912-15925.

[29]   YOO H I, SONG C R, LEE D K. Electronic carrier mobilities of $BaTiO_3$[J]. Journal of the European ceramic society, 2004, 24：1259-1263.

[30]   HSU H P, LI L C, SHELLAIAH M, et al. Structural, photophysical, and electronic properties of $CH_3NH_3PbCl_3$ single crystals[J]. Scientific reports, 2019, 9(1)：1-14.